Synthesis, characterization, and kinetic studies of multifunctionalized mesoporous silica for adsorption of zinc

Alime ÇITAK[*]

Department of Chemical Engineering, Faculty of Engineering and Architecture, Eskişehir Osmangazi University,
Eskişehir, Turkey

Abstract: The aim of this study is to evaluate the utilization of bifunctional mesoporous silica with a platinum and propylsulfonic acid group ($Pt/SBA15$-$PrSO_3H$) as an adsorbent for the removal of $Zn(II)$ ions from aqueous solutions. The SBA15-functionalized organosulfonic acid material was synthesized with a one-step cocondensation synthesis route. The second step was Pt loading during reduction and deposition into the aqueous suspension of the bifunctional mesoporous silica synthesized by an aqueous solution of formaldehyde as the reducing agent. The propylsulfonic acid and platinum functionalized mesoporous silica were characterized by BET, thermogravimetric analysis, and X-ray diffraction methods. The adsorption properties and thermodynamic parameters of the bifunctional mesoporous silica synthesized to adsorb $Zn(II)$ ions were studied. The effects of pH, initial concentration, temperature, adsorption equilibrium, and adsorption kinetics on the adsorption of zinc were investigated using the synthesized bifunctional mesoporous silica.

Key words: Bifunctionalized SBA15, metal adsorption, kinetic model, adsorption isotherm, mesoporous material

1. Introduction

The discharge of wastewater including toxic heavy metal ions into the environment is an increasing ecological problem. The toxic heavy metal ions consist mostly of Pb, Cr, Cu, Ni, and Zn. While these heavy metal ions may be found in nature, they are also released into the environment by industrial plants.[1] In the determination and/or removal of these metal ions from aqueous systems, adsorption is known as an especially effective, appropriate, easily applied, and economical process. Adsorbents such as molecular sieves, activated alumina, silica, and ion-exchange resins are usually used for separation of heavy metal ions from water.[2,3] Activated carbon is commonly used as an adsorbent to remove these metals from wastewater, although it has a high cost.[4] Thus, other alternative materials as cheaper adsorbents are being investigated to remove heavy metal ions from aqueous solutions. Mesoporous silica materials are among the most effective adsorbents for adsorption of pollutants from wastewater due to their advantageous properties such as large surface area, convenient porous diameter, and regular structure.[5−8] In addition, mesoporous silica materials can be modified with organic groups such as mercaptopropyl and aminopropyl to remove metal ions effectively. Recently, new hybrid organic-inorganic mesoporous-ordered structures, such as tannic acid-SBA-15 mesoporous nanocomposite, SBA-PAni, and SBA-15/PAMAM dendrimer hybrid, are widely investigated as adsorbents for the removal of metal ions and organic compounds such as dyes.[9−11]

Since the appearance of M41S, a silica-based mesoporous material, research has been initiated in the

---

[*]Correspondence: acitak@ogu.edu.tr

synthesis and characterization of various catalytic applications of mesoporous materials with high surface area and large and uniform pore size distribution (PSD). They have potential applications in the areas of catalysis, adsorption, and separation.[12,13] SBA15, one of these materials, has attracted considerable attention recently because it has larger pores, more pore walls, and higher hydrothermal stability than the commonly known MCM-41. To obtain the polymeric SBA15, templated silica is used with poly(ethylene oxide)-poly(propylene oxide)-poly(ethylene oxide), which has a biomaterial feature and is cheaper than MCM-41. MCM-41 is a surfactant-templated ordered mesoporous material.[12−14] SBA15 has another attractive feature, the existence of microspores interconnecting hexagonally ordered mesoporous. This feature makes SBA15 more suitable due to the diffusion inside the entire porous structure.[15]

Due to the discharge of heavy metals from both natural and human sources such as the chemical and electronics industries, the pollution of heavy metals in water resources has become a serious environmental problem in recent years. Heavy metal ions are also harmful to the human body, aquatic animals and plants, and agricultural crops. Elimination of heavy metals is difficult. Consequently, a considerable amount of attention has been devoted in the last decades to discharge and evaluation.[3−4,16] The most abundant harmful metals in wastewater discharge and liquid effluents from many industries are Zn^{2+}, Pb^{2+}, Cr^{3+}, Cu^{2+}, Cd^{2+}, Mn^{2+}, and Hg^{2+}.[4,17−20] Among these metals, high levels of zinc can result in a risk of pancreatic problems and can cause health problems such as hardening of the arteries, skin irritation, and stomach cramps. However, heavy metals (such as Cu^{2+}, Mn^{2+}, and Zn^{2+}) in small quantities are not harmful.[2,21] Zn^{2+} and Cu^{2+} heavy metal ions are among the most common ones in industrial waters (e.g., metal coatings, mining, and batteries).[22] The accumulation of Zn^{2+} is identified by the US Environmental Protection Agency as source of increased health risk.[23]

The heavy metal levels in industrial wastewater and other water sources must be decreased to the maximum permissible value. Therefore, effective precautions are required to prevent heavy metal pollution in the ecosystem. For this purpose, surface water is analyzed by different methods for the detection of heavy metals such as zinc, lead, iron, and chromium. The porous materials used for detection are chosen with respect to different key features such as analytical performance and sensitivity.[24−26]

Many conventional methods of remediation are used to remove heavy metals from wastewaters. These methods can be listed as electrochemical treatments, reverse osmosis, adsorption, and ion exchange.[3,27−30] Adsorption onto solid materials is a valuable technique because of its simplicity, high efficiency, and low cost.[31−34] Among adsorbents, activated carbon is commonly used in industrial wastewaters all over the world.[35−39] Because of the high cost of activated carbon, numerous scientific studies have been conducted to find effective and low-cost adsorbents that can be used to effectively remove zinc. New hybrid organic-inorganic mesoporous ordering processes have been extensively studied as adsorbents for the removal of metal ions and organic contaminants. The large pores of SBA-15 can be combined with organic groups in a compatible behavior; the adsorption capacity can thus be increased considerably by means of active centers. In this study, SBA-15 was used for its large effective surface area functionalized with propylsulfonic acid and platinum due to the presence of active functional groups in the structure.[9]

The highlight of this paper is to evaluate organosulfonic acid-functionalized mesoporous silica SBA-15 (Pt/SBA15-PrSO$_3$H) as an alternative adsorbent to activated carbon, which has a high cost, for the removal of Zn(II) ions from aqueous solutions.[23] For this purpose, SBA-15-functionalized organosulfonic acid materials were synthesized via a one-step cocondensation synthesis route as described previously.[40−42] The second step

was Pt loading during reduction and deposition into the aqueous suspension of the bifunctional mesoporous silica synthesized by an aqueous solution of formaldehyde as the reducing agent. The propylsulfonic acid and platinum functionalized mesoporous silica (Pt/SBA15-PrSO$_3$H) were characterized by powder X-ray diffraction (XDR), Brunauer–Emmett–Teller (BET) surface area and PSD determination, and thermogravimetric analysis (TGA) methods. To observe the effect of temperature on the adsorption capacity of Pt/SBA15-PrSO$_3$H for zinc, different temperatures of 25 °C, 35 °C, and 45 °C were applied in the tests. The adsorption kinetics were studied to explain the adsorption mechanism. The experimental adsorption data were expressed using many adsorption isotherm models such as Langmuir and Freundlich as the most frequently used models.

2. Results and discussion

2.1. Characterization and physicochemical properties of modified SBA15

The powder XRD data by low angle are recorded in Figure 1 for SBA15 and bifunctional SBA15 (Pt/SBA15-PrSO$_3$H). The bifunctional SBA15 material has three diffraction peaks, one very intense peak and two weak peaks, which are indexable as (100), (110), and (200) diffractions with the ordered 2D hexagonal mesostructure. As a result, the structure of silica does not crack upon surface modification. The pore crystalline structures in the samples are perfectly retained when incorporating Pt and the organosulfonic acid.[43]
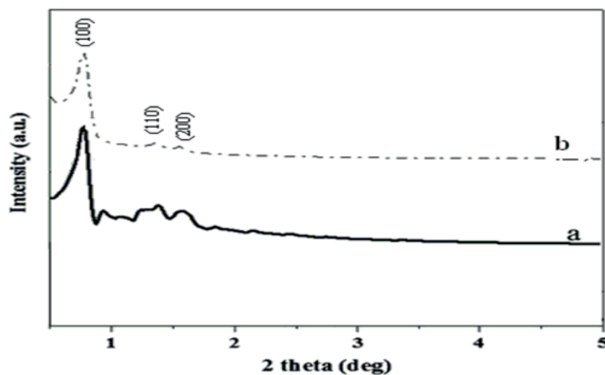

Figure 1. Powder XRD patterns of the catalyst samples: a) SBA15, b) Pt/SBA15-PrSO$_3$H.

The textural characteristics of the SBA-15 and bifunctional SBA-15 materials were analyzed by nitrogen adsorption at 77 K following the BET procedure. It was observed that the typical adsorption isotherm of the SBA-15 material was of type IV in nature as per IUPAC classification. The average pore diameter of the materials was calculated by the Barrett–Joyner–Halenda (BJH) method using the adsorption branch of the N$_2$ adsorption-desorption isotherms. BET surface area and average pore diameter of SBA-15 were calculated as 784 m^2 g^{-1} and 74.384 Å, respectively.

Figures 2 and 3 illustrate the N$_2$ adsorption-desorption isotherm and the pore size distribution of the Pt/SBA15-PrSO$_3$H used as an adsorbent for the removal of Zn(II) ions from aqueous solutions. The textural properties of the bifunctional catalyst are summarized in Table 1. The sample had type IV hysteresis loops with sharp adsorption and desorption curves according to the IUPAC classification as seen in Figure 2.[44] The BET surface area of the bifunctional catalyst is slightly smaller than that of pure SBA-15. The fall in surface area of the bifunctional catalyst used as an adsorbent may be due to the bifunctional (platinum and propylsulfonic acid) group that blocks the mesopores. When compared to pure SBA-15, the average pore diameter value of

bifunctional catalyst used as an adsorbent (69.693 Å) was found to be lower. The average pore diameter value of the bifunctional catalyst is found to decrease with the bifunctional group in the framework.
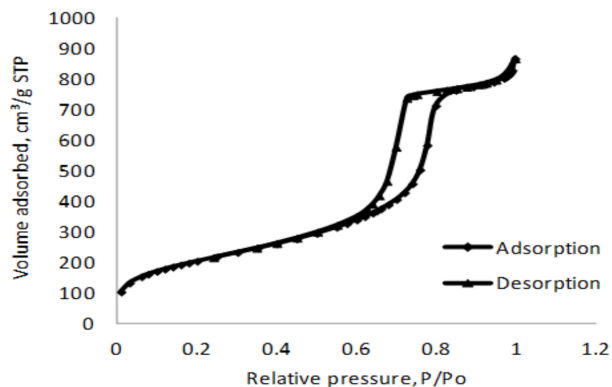

Figure 2. Nitrogen sorption isotherms of the Pt/SBA15-PrSO$_3$H material.
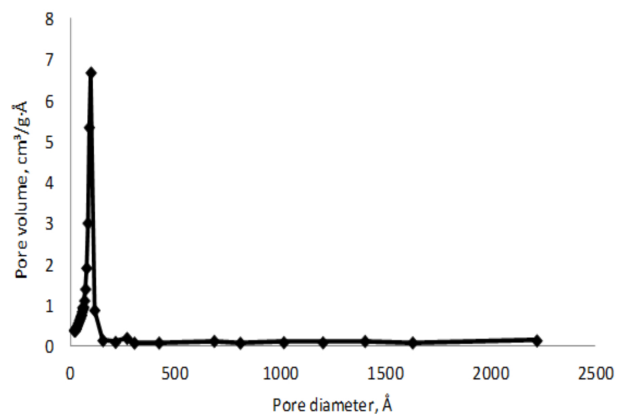

Figure 3. Pore size distributions of the Pt/SBA15-PrSO$_3$H material.

The rate of weight changes in TGA refers to the thermal stability of the material, the amount of moisture and solvent, and the percentage of the components of the organic loading on the silica framework.[45] In this work, it was observed that the thermal stability of the catalysts (pure and bifunctional) was very high as a result of TGA. The desorption of the physically adsorbed water was below 100 °C. The TGA results showed that the weight loss of the pure SBA-15 material was constant up to 700 °C. The TGA results for the prepared Pt/SBA15-PrSO$_3$H bifunctional catalyst are represented in Figure 4. The weight loss at around 460 °C indicated the presence of propylsulfonic acid groups.[46]

2.2. Heavy metal ion adsorption studies

2.2.1. Influence of pH

The initial pH value of the aqueous solution is an important variable in all processes. Figure 5 illustrates the influence of initial pH on percentage removal of zinc ion concentration of 50 ppm and shaking time of 6 h onto mesoporous material (Pt/SBA15-PrSO$_3$H). As seen in Figure 5, the percentage removal increases between pH 3.08 and 7.98. Then the percentage removal of zinc ion suddenly increased to 95% when the initial pH value of the aqueous solution was 7.98. This may be due to the formation of aggregates. Generally, ZnO nanoparticles begin with a reaction between zinc chloride (zinc precursor) and hydroxide ions, followed by an aggregation process. They will aggregate a lot after the synthesis is done. Therefore, the initial pH value of the aqueous solution is important. For avoiding the precipitation of metals, pH 7.05 was chosen as the optimum pH value for maximum intake of Zn.

2.2.2. Influence of the mesoporous silica dosage

In the experimental studies applied to determine the optimum adsorbent dosage, the adsorbent dosage was varied from 0.01 to 0.13 g per 50 mL. Figure 6 shows that the percentage removal of zinc ions at a Zn^{2+} concentration of 50 ppm increases with increasing adsorbent dosage. This can be explained by the increase in the surface area of the adsorbent. In this study, adsorbent dosage was chosen to be 0.1 g per 50 mL for the removal of zinc.
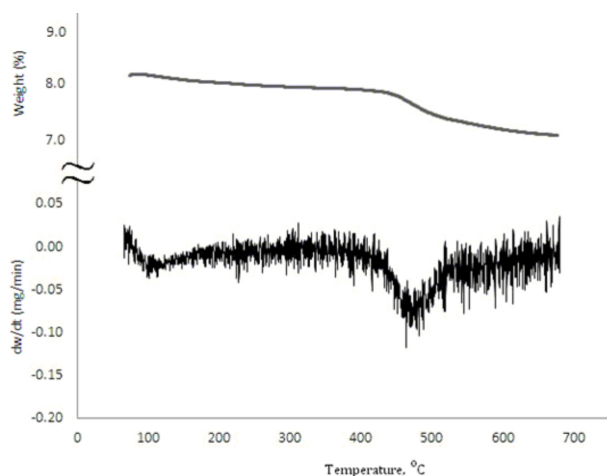
Figure 4. TGA and DTA analyses of the functionalized mesoporous silica, Pt/SBA15-PrSO$_3$H.
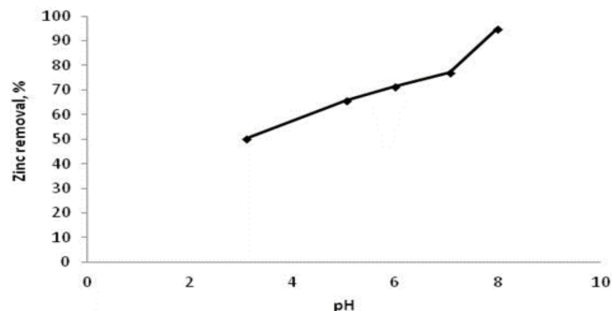

Figure 5. Influence of pH on the adsorption of metal ion onto Pt/SBA15-PrSO$_3$H.

2.3. Kinetic modeling

The kinetics of Zn^{2+} adsorption onto Pt/SBA15-PrSO$_3$H were studied to determine the adsorption mechanism.

2.3.1. Pseudo-first-order model

The rate constant of adsorption was calculated from the pseudo-first-order rate equation given by Lagergreen[47] and Ho:[48]

$$\log (q_e - q_t) = \log q_e - \frac{k_1}{2.303}t \tag{1}$$

where k_1 is the rate constant of adsorption (min^{-1}), q_t is the zinc metal dosage adsorbed at any time t (mg g^{-1}), and q_e is the zinc metal dosage adsorbed at saturation time (mg g^{-1}).

To calculate the values of k_1 and q_e for zinc, the first-order reaction kinetic model was tested. The curve in the plots of the log ($q_e - q_t$) against time was linear, which can be obtained from the slope and intercept of the plot (Figure 7). The calculated k_1, q_e, and linear regression correlation coefficient (R^2) values are listed in Table 2.
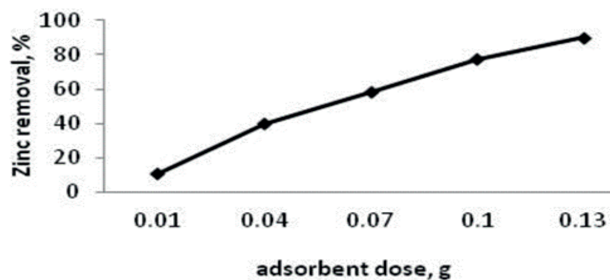

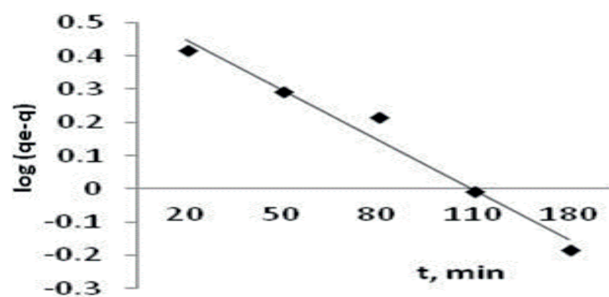**Figure 6**. Influence of adsorbent dose on the percentage removal of metal ion (25 °C, C$_o$: 50 mg L^{-1}, pH 7.05).

Figure 7. Pseudo-first-order kinetic model.

Table 1. Textural properties of the Pt/SBA15-PrSO$_3$H.

Textural properties		
BET (m^2 g^{-1})	BJH ads. average pore diameter (Å)	Ads. total pore volume V$_T$ (cm^3 g^{-1})
745.12	69.693	1.268

2.3.2. Pseudo-second-order model

The rate constant of adsorption was determined from the following pseudo-second-order rate expression given by Ho and McKay:[49]

$$\frac{t}{q_t} = \frac{1}{k_2 q_e^2} + \frac{1}{q_e}t, \tag{2}$$

where k$_2$ is the adsorption rate constant for the second-order adsorption (g mg^{-1} min^{-1}).

To calculate the values of k$_2$ and q$_e$ for zinc, the second-order reaction kinetic model was tested. The curve in the plots of the t/q$_t$ against time was linear, which can be obtained from the slope and intercept of the plot (Figure 8). The calculated k$_2$, q$_e$, and R^2 values are listed in Table 2.
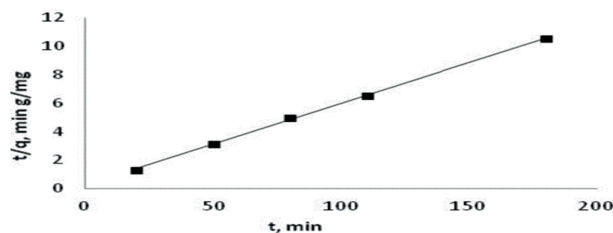

Figure 8. Pseudo-second-order kinetic model.

Table 2 lists k$_1$, k$_2$, q$_e$ (calculated), and q$_e$ (experimental) for the zinc metal ions at an initial concentration of 50 mg L^{-1}. The q$_e$ value calculated from the pseudo-first-order kinetic model was not close to the experimental q$_e$ value. However, in the pseudo-second-order kinetic model, the calculated q$_e$ is close to the experimental q$_e$ value for the zinc metal ions. The R^2 value of the pseudo-second-order model was better than in the pseudo-first-order model. The pseudo-second-order model is therefore more acceptable than the pseudo-first-order model.

2.3.3. Comparison of adsorption isotherms

The equilibrium data were well fitted using two of the most commonly used isotherms that are known to search for the relationship between solid and liquid equilibrium concentration systems, as given by Eqs. (3) and (4).[50]

The Langmuir and Freundlich isotherm models are represented by the following equations, respectively:

$$\frac{C_e}{q_e} = \frac{1}{q_o b} + \frac{C_e}{q_o}, \tag{3}$$

$$log q_e = log k_f + \frac{1}{n} \log C_e, \tag{4}$$

where the constant q_o denotes the capacity of the monolayer adsorption (mg g^{-1}) and b is related to the energy of sorption (L mg^{-1}). k_f and n are the Freundlich adsorption isotherm constants related to the adsorption capacity and intensity of adsorption, respectively.

The Freundlich sorption isotherm is given for adsorption on heterogeneous surfaces, indicating a multilayer sorption of active sites on the surface, while the Langmuir isotherm expresses a single coating layer on the surface.

The linearized forms of the Langmuir and Freundlich isotherms given by Eqs. (3) and (4), respectively, can be seen in Figures 9 and 10 for zinc metal adsorption onto Pt/SBA15-PrSO$_3$H mesoporous material. The values of the adsorption coefficients, which are the Langmuir equilibrium constant b, Langmuir monolayer adsorption capacity q_o, adsorption intensity n, and Freundlich constant k_f, are computed from the plots of these isotherms and are listed in Table 3.
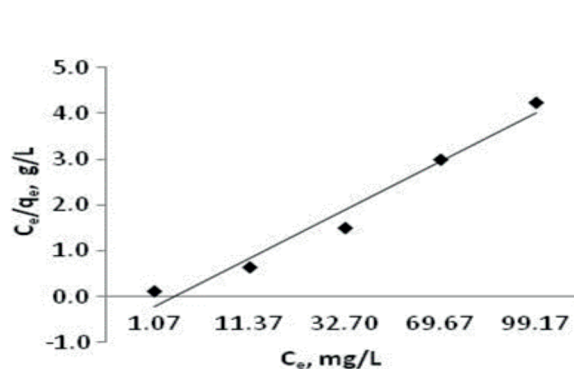

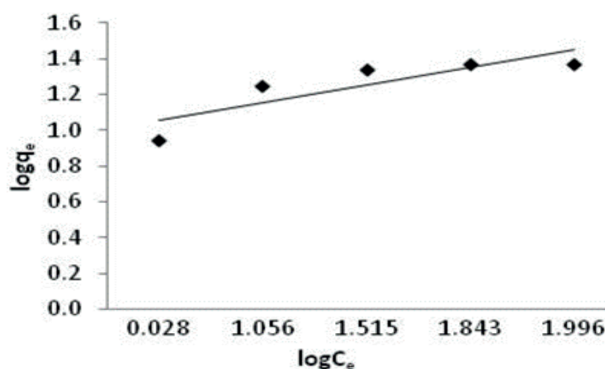**Figure 9**. Langmuir plot for the adsorption of metal ion onto Pt/SBA15-PrSO$_3$H.

Figure 10. Freundlich plot for the adsorption of metal ion onto Pt/SBA15-PrSO$_3$H by Pt/SBA15-PrSO$_3$H.

Table 2. The kinetic parameters for the adsorption of metal ions on the Pt/SBA15-PrSO$_3$H mesoporous material.

Pseudo-first-order constants			Pseudo-second-order constants			Experimental
q_e (mg g^{-1})	k_1 (L min^{-1})	R^2	q_e (mg g^{-1})	k_2 (g mg^{-1} min^{-1})	R^2	q_e (mg g^{-1})
3.96	0.3461	0.973	17.48	0.0121	0.999	23.38

Table 3. Adsorption isotherm model parameters for the adsorption of Zn(II) onto Pt/SBA15-PrSO$_3$H.

Langmuir			Freundlich		
q_o (mg g^{-1})	b (L mg^{-1})	R^2	k_f (mg g^{-1})	n	R^2
0.9428	−0.8295	0.9685	9.1264	10.277	0.7222

The results of Table 3 show a significant correlation between the experimental data and the theoretical data predicted by the Langmuir isotherm model. The adsorption isotherm of Zn^{2+} exhibits Langmuir behavior, which expresses a monolayer adsorption. It is seen that the Langmuir isotherm model fits very well with the experimental results for Zn^{2+} metal adsorption from aqueous solutions using Pt/SBA15-PrSO$_3$H bifunctional material.

2.3.4. Influence of initial metal ion concentration

Figure 11 shows the influence of various initial zinc concentrations (20–150 mg Zn^{2+} L^{-1}) on the Pt/SBA15-$PrSO_3H$ under the optimum contact time of 6 h and 0.1 g of adsorbent per 50 mL of solution at pH 7.0 and 25 °C. The results show that the adsorption of the metal ions takes place quickly until 80 mg L^{-1} Zn^{2+} concentration is reached. Then it is almost stable in the 100 and 150 mg Zn^{2+} L^{-1} concentration range. The maximum adsorption efficiency was determined as 50 mg Zn^{2+} L^{-1} for the Pt/SBA15-$PrSO_3H$ bifunctional mesoporous material.

2.3.5. Influence of temperature on the metal ion adsorption onto Pt/SBA15-$PrSO_3H$

To study the influence of adsorption temperature on the metal adsorption capacity onto the Pt/SBA15-$PrSO_3H$ surface, the experiments were performed with the initial zinc metal ion concentration of 50 mg L^{-1} at 6 h of contact time and 0.1 g of adsorbent amount for three different temperatures of 25 °C, 35 °C, and 45 °C with constant stirring speed of 140 rpm. The plot of zinc removal % versus temperature is shown in Figure 12. The increase in the adsorption rate may be due to the strong attractive forces between the active sites of the mesoporous material and zinc ions. A slight increase was obtained in Zn(II) sorption on the bifunctional mesoporous material by increasing the temperature of the system. Thus, the adsorption of metal ion onto the Pt/SBA15-$PrSO_3H$ surface was an endothermic process.[1,51]
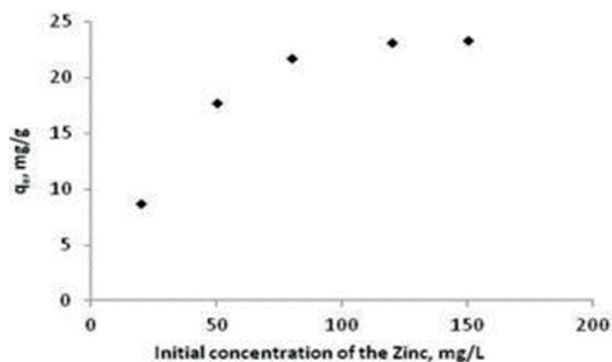

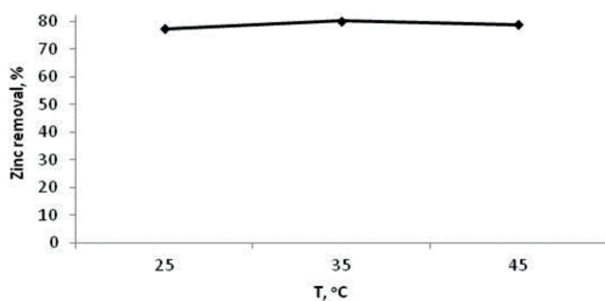**Figure 11**. Influence of initial metal ion concentration on the removal of metal ion.

Figure 12. Influence of temperature on the adsorption of metal ion onto Pt/SBA15-$PrSO_3H$.

2.3.6. Thermodynamics studies

The thermodynamic parameters (such as Gibbs free energy ($\Delta G°$), entropy ($\Delta S°$) and enthalpy ($\Delta H°$)) for the adsorption of zinc on the mesoporous material were calculated by using the following equation:

$$\Delta G° = -RT \ln K, \tag{5}$$

according to the van't Hoff equation:

$$\ln K = \left(\frac{\Delta S°}{R} \right) - \left(\frac{\Delta H°}{RT} \right), \tag{6}$$

$$\Delta G = \Delta H - T\Delta S, \tag{7}$$

where R is the ideal gas constant, K is the equilibrium constant, and T is the temperature in Kelvin.

The independence of the enthalpy change from temperature was assumed in the temperature range applied. The values of the enthalpy ($\Delta H°$, kJ mol^{-1}) and the entropy ($\Delta S°$, J mol^{-1} K^{-1}) are obtained from the lnK versus 1/T plot using Eq. (6), as given in Figure 13. The Gibbs free energy (ΔG) is calculated using well-known Eq. (5). The thermodynamic parameters for the adsorption of metal ions onto Pt/SBA15-PrSO$_3$H at pH 7.0 with adsorbent dosage of 0.1 g per 50 mL are listed in Table 4. The small positive value of enthalpy change ΔH shows the endothermic nature of the metal ion adsorption. ΔH_{ads} is the enthalpy change because of the chemisorption of metal complexes and new bond formations at the sorbent surface in chemisorption, and as a result, ΔH_{ads} can be slightly positive.[52] Also, the small positive value of entropy change ΔS shows that the system does not have random behavior. It is shown that the values of free energy change (ΔG) of the system are negative, as expected for adsorption processes.[24]
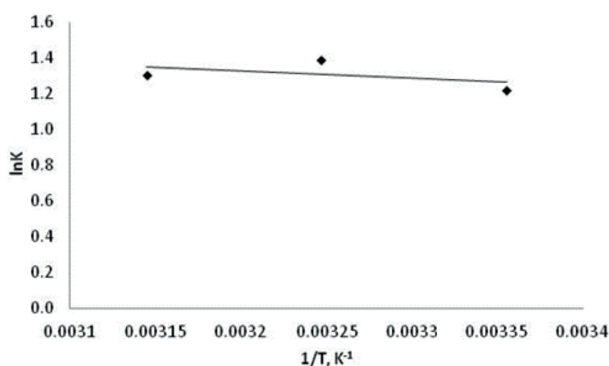

Figure 13. lnK versus 1/T (0.1 g Pt/SBA15-PrSO3H, C$_o$: 50 mg/L, pH 7.0).

Table 4. Thermodynamic parameters for the adsorption of metal ion onto Pt/SBA15-PrSO$_3$H, pH 7.0.

Temperature (K)	$\Delta G°$ (kJ mol^{-1})	$\Delta H°$ (kJ mol^{-1})	$\Delta S°$ (J mol^{-1} K^{-1})	K
298	−3.029			3.396
308	−3.565	3.369	21.81	4.024
318	−3.451			3.689

2.3.7. Desorption studies

Desorption studies of Zn(II) ions are key processes to measure the facility of recycling of adsorbents. Desorption experiments were carried out by treating 0.1 g of Pt/SBA15-PrSO$_3$H with adsorbed Zn(II) ions. A solution of 2 M HCl, 0.05 M EDTA, and 1 M NaCl was used as a complexing agent. When 2 M HCl solution was used, the desorbed zinc(II) metal ions were able to replace H$^+$ ions onto Pt/SBA15-PrSO$_3$H. The adsorbent was filtered and the final concentration of the liquid that passed through the filter was analyzed to determine the desorbed zinc(II) ions by atomic absorption spectrophotometer (AAS). The desorption of zinc(II) metal ions was 47.5% for all complexing agents and the results were obtained from an AAS analyzer.

3. Experimental

3.1. Chemicals

The tetraethyl orthosilicate (TEOS) (98%, Aldrich) and 3-mercaptopropyltrimethoxysilane (MPTMS) (85%, Acros) were used as the silica precursor and the organosulfonic acid source, respectively. Pluronic P123 (BASF),

a triblock copolymer of polyethyleneoxide–polypropyleneoxide–polyethyleneoxide with the molecular structure of PEO20–PPO70–PEO20 (Mw = 5800), was used as the template material to make up the structural properties of the mesoporous materials. An aqueous solution of $PtCl_4$ (platinum(IV) chloride) (Acros) and formaldehyde (HCHO) (37%, Fisher) were used as the platinum precursor and the reducing agent, respectively.

3.2. Synthesis of Pt/SBA15-PrSO$_3$H

Pluronic P123, a triblock copolymer of polyethylene oxide–polypropylene oxide–polyethylene oxide (PEO20–PPO70–PEO20; Mw = 5800), was used as the template material. Tetraethoxysilane (TEOS, 98%) as the silica precursor and 3-mercaptopropyl trimethoxysilane (MPTMS, 85%) as the organosulfonic acid source were used in synthesis. Also, 0.01 g Pt mL^{-1}, an aqueous solution of platinum(IV) chloride ($PtCl_4$) as the platinum precursor, and an aqueous solution of formaldehyde (HCHO, 37%) as the reducing agent were used. This synthesized catalyst was identified as a bifunctional catalyst.

The catalyst used in this work is a bifunctional organic-inorganic hybrid SBA15 material loaded with two stages, propylsulfonic acid and platinum, respectively. The weight percentage of platinum in the catalysts was 1% and the molar ratio of organosulfonic acid precursor/TEOS was kept at 10% for all the experimental works to prepare the catalyst. For synthesizing the Pt/SBA15-PrSO$_3$H bifunctional catalyst, a two-step procedure was used. In the first step, organosulfonic acid-functionalized mesoporous silicas were synthesized according to a method described previously.[41] In the second step, an aqueous solution of platinum(IV) chloride ($PtCl_4$) was added into the aqueous phase of SBA15-PrSO$_3$H, which is 1 g of SBA15-PrSO$_3$H with the corresponding amount of Pt in deionized water (0.01 g Pt mL^{-1}) with vigorous stirring. The color of the suspension changed from yellow to black, indicating the reduction of Pt^{4+} to Pt^0 with stirring for 24 h at 60 °C. Formaldehyde was used as the reducing agent. The sample was filtered, washed with deionized water, and vacuum-dried overnight at 100 °C after cooling to room temperature.[53,54]

3.3. Catalyst characterization

The surface area and porosity of the catalyst were determined by N_2 adsorption-desorption measurements at 77 K (–196 °C) using a Micromeritics ASAP 2020 apparatus. The surface area, pore volume, and PSD were determined using the BET and BJH methods, respectively. The surface area was measured in the linear relative pressure range between 0.01 and 0.99. Before the measurement, the sample was degassed at 100 °C for 5 h.

The prepared Pt/SBA15-PrSO$_3$H bifunctional catalyst was identified by powder XRD patterns acquired on a Rigaku Rota?ex D/Max-C X-ray diffractometer using Cu Kα radiation at 40 kV and 120 mA. The data were obtained from 0.5 to 5° (2θ) using a step size of 0.02°.

The organic composition and thermal stability of the modified mesoporous material were determined by TGA and differential TGA methods using a PerkinElmer TGA7 instrument model. The thermograms were obtained by heating from 42 to 670 °C at the rate of 10 °C min^{-1} under air flow.

3.4. Adsorption testing

Batch-wise adsorption studies were carried out in 100-mL stirred flasks for 48 h in a temperature-controlled water bath with a shaker (MEMMERT) set to 140 rpm at constant temperature. In batch adsorption experiments, 0.01 g of the adsorbent was put in capped volumetric flasks with 50 mg L^{-1} of aqueous Zn^{2+} solution. After the

completion of the adsorption process, the samples were centrifuged at 5000 rpm for 10 min. The zinc amounts in the supernatant solutions were determined spectrophotometrically using a Hach DR-2000 spectrophotometer. The concentration of zinc ions left in the bulk solution in the desorption experiments was determined using the AAS technique (PerkinElmer, Analyst A400). To investigate the pH effects on zinc adsorption, different pH levels (3.08–7.98) of the $ZnCl_2$ solutions were adjusted by adding 0.1 N NaOH and HCl solutions and were measured using a pH-meter (Ino Lab). The study of the adsorbent doses was conducted using different amounts of adsorbents (0.01–0.13 g). The effect of initial zinc concentration at pH 7.0 was investigated at different concentrations (20–150 mg Zn^{2+} L^{-1}) and 25 °C. The experiments were performed at temperatures of 25 °C, 35 °C, and 45 °C to determine the effect of temperature under isothermal conditions. To determine the adsorption capacity of the adsorbent, the Langmuir and Freundlich isotherm models were employed. The batch adsorption kinetics experiments were performed in an agitated flask with constant initial Zn^{2+} concentration value (50 mg L^{-1}). The retention times were varied from 5 to 180 min at 25 °C with pH 7.0.

References

1. Sheela, T.; Nayaka, Y. A.; Viswanatha, R.; Basavanna, S.; Venkatesha, T. G. *Powder Technol.* **2012**, *217*, 163-170.

2. Aragay, G.; Pons, J.; Merkoçi, A. *Chem. Rev.* **2011**, *111*, 3433-3458.

3. Hajiaghababaei, L.; Badiei, A.; Ganjali, M. R.; Heydari, S.; Khaniani, Y.; Ziarani, G. M. *Desalination* **2011**, *266*, 182-187.

4. Jeon, E. Y.; Ansari, M. B.; Mo, Y. H.; Park, S. E. *J. Hazard. Mater.* **2011**, *185*, 1311-1317.

5. Kanthasamy, R.; Mbaraka, I. K.; Shanks, B. H.; Larsen, S. C. *Appl. Magn. Reson.* **2007**, *32*, 513-526.

6. Yuan, Q.; Li, N.; Chi, Y.; Geng, W. C.; Yan, W. F.; Zhao, Y.; Li, X. T; Dong, B. *J. Hazard. Mater.* **2013**, *254-255*, 157-165.

7. Yun, L.; Chaonan, H.; Jiajia, Y.; Junyu, P.; Jing, J.; Huilian, M.; Jiping, C. *J. Chromatogr. A* **2017**, *1527*, 10-17.

8. Wan, X.; Yao, S.; Liu, H.; Yao, Y. *J. Mater. Chem. A* **2013**, *1*, 10505-10512.

9. Aghajani, K.; Tayebi, H. A. *Fiber. Polym.* **2017**, *18*, 465-475.

10. Tafti, A. G.; Rashidi, A.; Tayebi, H. A.; Yazdanshenas, M. E. *Int. J. Nano Dimens.* **2018**, *9*, 79-88.

11. Mirzaie, M.; Rashidi, A.; Tayebi, H. A.; Yazdanshenas, M. E. *J. Polym. Environ.* **2018**, *26*, 1831-1843.

12. Xue, X.; Li, F. *Micropor. Mesopor. Mater.* **2008**, *116*, 116-122.

13. Jana, S. K.; Takahashi, H.; Nakamura, M.; Kaneko, M.; Nishida, R.; Shimizu, H.; Kugita, T.; Namba, S. *Appl. Catal. A-Gen.* **2003**, *245*, 33-41.

14. Zhao, D.; Feng, J.; Huo, Q.; Melosh, N.; Fredrickson, G. H.; Chmelka, B. F.; Stucky, G. D. *Science* **1998**, *279*, 548-552.

15. Wenjie, Z.; Jingxuan, W.; Di, W.; Xitong, L.; Yongming, L.; Caiyun, H.; Wenhui, M.; Sufang, H. *Nanoscale Res. Lett.* **2017**, *12*, 1-9.

16. Malkoc, E.; Nuhoglu, Y. *J. Hazard. Mater.* **2005**, *127*, 120-128.

17. Veli, S.; Akyüz, B. *J. Hazard. Mater.* **2007**, *149*, 226-233.

18. Rafatullaha, M.; Sulaiman, O.; Hashim, R.; Ahmad, A. *J. Hazard. Mater.* **2009**, *170*, 969-977.

19. Liu, S. Y.; Gao, J.; Yang, Y. J.; Yang, Y. C.; Ye, Z. X. *J. Hazard. Mater.* **2010**, *173*, 558-562.

20. Wang, L.; Qi, T.; Zhang, Y. *Colloids Surf. A Physicochem. Eng. Asp.* **2006**, *275*, 73-78.

21. EPA. *EPA-738-F-92-007*; US Environmental Protection Agency: Washington, DC, USA, 1992.

22. Cheremisinoff, P. N. *Handbook of Water and Wastewater Treatment Technology*; Marcel Dekker: New York, NY, USA, 1995.

23. Jain, C. K.; Singhal, D. C.; Sharma, M. K. *J. Hazard. Mater. B* **2004**, *114*, 231-239.

24. Kocaoba, S. *J. Hazard. Mater.* **2007**, *147*, 488-496.

25. Wu, Z.; Zhao, D. *Chem. Commun.* **2011**, *47*, 3332-3338.

26. Li, G.; Zhao, Z.; Liu, J.; Jiang, G. *J. Hazard. Mater.* **2011**, *192*, 277-283.

27. Bektas, N.; Agim, B. A.; Kara, S. *J. Hazard. Mater. B* **2004**, *112*, 115-122.

28. Ozcan, A. S.; Gok, O.; Ozcan, A. *J. Hazard. Mater. B* **2009**, *161*, 499-509.

29. Feng, X.; Fryxell, G. E.; Wang, L. Q.; Kim, A. Y.; Liu, J.; Kemner, K. M. *Science* **1997**, *276*, 923-926.

30. Monteagudo, J. M.; Ortiz, M. J. *J. Chem. Technol. Biotechnol.* **2000**, *75*, 767-772.

31. Mureseanu, M.; Reiss, A.; Stefanescu, I.; David, E.; Parvulescu, V.; Renard, G.; Hulea, V. *Chemosphere* **2008**, *73*, 1499-1504.

32. Yang, L. M.; Wang, Y. J.; Luo, G. S.; Dai, Y. Y. *Micropor. Mesopor. Mat.* **2005**, *84*, 275-282.

33. Liu, A. M.; Hidajat, K.; Kawi, S.; Zhao, D. Y. *Chem. Commun.* **2000**, *13*, 1145-1146.

34. Yang, Q. H.; Liu, H.; Yang, H.; Zhang, L.; Feng, Z. C.; Zhang, J.; Li, C. *Micro. Mesop. Mater.* **2005**, *77*, 257-264.

35. Pujol, L.; Evrard, D.; Groenen-Serrano, K.; Freyssinier, M.; Ruffien-Cizsak, A.; Gros, P. *Front. Chem.* **2014**, *2*, 1-24.

36. Ramos, R. L.; Jacome, L. A. B.; Barron, J. M.; Rubio, L. F.; Coronado, R. M. G. *J. Hazard. Mater. B* **2002**, *90*, 27-38.

37. Veli, S.; Öztürk, T. *Fresenius Environ. Bull.* **2005**, *14*, 212-218.

38. Ferro-García, M. A.; Rivera-Utrilla, J.; Rodríguez-Gordillo, J.; Bautista-Toledo, I. *Carbon* **1988**, *26*, 363-373.

39. Sierra, I.; Pérez-Quintanilla, D. *Chem. Soc. Rev.* **2013**, *42*, 3792-3807.

40. Thu, P. T. T.; Thanh, T. T.; Phi, H. N.; Vo, V. *J. Mater. Sci.* **2010**, *45*, 2952-2957.

41. Mbaraka, I. K.; Shanks, B. H. *J. Catal.* **2005**, *229*, 365-373.

42. Morales, V.; Idso, M. N.; Balabasquer, M.; Chmelka, B.; García-Mun oz, R. A. *J. Phys. Chem. C* **2016**, *120*, 16887-16898.

43. Tang, Y.; Miao, S.; Mo, L.; Zheng, X.; Shanks, B. H. *Top. Catal.* **2013**, *56*, 1804-1813.

44. Tang, Y.; Miao, S. Shanks, B. H.; Zheng, X. *Appl. Catal. A-Gen.* **2010**, *375*, 310-317.

45. Kureshy, R. I.; Ahmad, I.; Pathak, K.; Khan, N. H.; Abdi, S. H. R.; Jasra, R. V. *Catal. Commun.* **2009**, *10*, 572-575.

46. Buchmeiser, M. R. *Polymeric Materials in Organic Synthesis and Catalysis*; Wiley-VCH: Weinheim, Germany, 2003.

47. Mirzaie, M.; Rashidi, A.; Tayebi, H. A.; Yazdanshenas, M. E. *J. Chem. Eng. Data* **2017**, *62*, 1365-1376.

48. Miao, S.; Shanks, B. H. *Appl. Catal. A-Gen.* **2009**, *359*, 113-120.

49. Lagergreen, S. K. *Sven. Vetenskapsakad. Handl.* **1898**, *24*, 39.

50. Ho, Y. S. *Scientometrics* **2004**, *59*, 171-177.

51. Ho, Y. S.; McKay, G. *Chem. Eng. J.* **1998**, *70*, 115-124.

52. Rao, M.; Parwate, A. V.; Bhole, A. G. *Waste Manage.* **2002**, *22*, 821-830.

53. Sen, T. K.; Gomez, D. *Desalination* **2011**, *267*, 286-294.

54. Iman, A., Yazdanshenas, M. E., Tayebi, H.A.; Nasirizadeh, N. *Physical Chemistry Research* **2017**, *5*, 659-679.